This article has been accepted for publication in a future issue of this journal, but has not been fully edited. Content may change prior to final publication. Citation information: DOI 10.1109/LAWP.2016.2590477, IEEE Antennas and Wireless Propagation Letters

A Miniaturized CSRR Loaded Wide-Beamwidth Circularly Polarized Implantable Antenna for Subcutaneous Real-Time Glucose Monitoring

XiongYing Liu, *Member*, *IEEE*, ZeTao Wu, Yi Fan, and Manos M. Tentzeris, *Fellow*, *IEEE*

***Abstract*—A single-fed miniaturized wide-beamwidth circularly polarized implantable antenna, operating in the industrial, scientific and medical (ISM) band (2.40–2.48 GHz), is designed and experimentally verified for subcutaneous real-time glucose monitoring applications. The proposed antenna features a very good miniaturization with the dimensions of 8.5 × 8.5 × 1.27 mm^3 by employing four C-shaped slots and a complementary split-ring resonator (CSRR). Meanwhile, by adjusting the slits of CSRR, circular polarization (CP) is realized. The simulation results in a three-layer phantom demonstrate that the impedance bandwidth is 12.2% (2.32–2.62 GHz) with a peak gain of -17 dBi and the 3-dB axial ratio (AR) bandwidth is 2.4% (2.42–2.48 GHz) with a wide beamwidth of around 140°. An in-vitro test was carried out in a pork slab and the measured impedance bandwidth is 13% (2.31–2.63 GHz) with S_{11} < -10 dB, confirming the simulated results. The Specific Absorption Rate (SAR) distribution has been evaluated for the consideration of health safety and the calculated link margin shows that the reliable communication can be guaranteed within 10 m in free space.**

***Index Terms*—Circular polarization (CP), complementary split ring resonator (CSRR), glucose monitoring, implantable antennas, link margin, wide beamwidth.**

I. Introduction

FOR DIABETIC patients, glucose concentrations should be controlled in an appropriate range. Subcutaneous glucose sensors can be adopted to continuously monitor the glucose level in real time [1], [2]. However, to be truly beneficial, these sensors should have the ability to communicate wirelessly and reliably with external devices. Therefore, an integrated antenna is necessary to transmit the physiological information from the body-implantable sensors to outside receivers wirelessly [3].

Due to the stringent limitations for body-implantable devices, it is a great challenge to design the implantable antennas with the appropriate characteristics of biocompatibility, miniaturization, safety, and reliable communications [4]. The relevant miniaturization techniques for implantable antennas include, but are not limited to, the use of high permittivity substrates, fractal structures [5], and shorting pins loading [6]. Recently, the synthesized metamaterial particle SRR and its dual CSRR [7] have been employed for the microwave component miniaturization as they can effectively realize a negative permeability or permittivity [8]. Due to common human tissue activities and posture movements, it is virtually impossible for the in-body antennas to maintain a fixed orientation relatively to external receivers. To alleviate these issues and guarantee a robust data communication, the adoption of circularly polarized antennas with a wide beamwidth would be an excellent solution due to their inherent immunity to time-varying orientations between the transmitters and the receivers. Despite the above advantage, only very few researchers have focused on the design of miniaturized implantable CP antennas. In [9], a capacitively loaded CP implantable patch antenna for biomedical applications was designed with a significantly large size and a very narrow bandwidth. Another CP implantable antenna for an ingestible capsule endoscope was developed in [10], featuring an even larger size.

In this work, a novel miniaturized CP implantable antenna is proposed for subcutaneous glucose monitoring operating in the ISM band of 2.40–2.48 GHz. Four C-shaped slots and a CSRR loading the radiation patch are employed to enable miniaturization. In addition, by adjusting the slits of the CSRR, a reliable CP with a wide beamwidth is achieved.

This letter is organized as follows. Section II illustrates the configuration of the proposed implantable antenna along with preliminary simulation results and a discussion of its operation principle. Section III discusses the in-vitro results and the link margin estimation, while the conclusions are given in Section IV.

II. Antenna Design and Discussion

A. Antenna Design

The structure of the proposed CP antenna is shown in Fig. 1. For proof-of-concept demonstration purposes, a prototype is etched on a substrate of Rogers 3210 (ε_r = 10.2, tan δ = 0.003) and covered with the same layer. Each layer has the same thickness of 0.635 mm. A circular CSRR, composed of two concentric metallic slot rings on which two small slits are cut in opposite directions, is printed in the center of the radiation patch. Besides, the patch is surrounded by four C-shaped slots.

This work was supported in part by the National Natural Science Foundation of China under Grant 61372008, 61327005 and in part by the GDSTC under Grant 2014A010103014, 2015B010101006.

X. Y. Liu, Z. T. Wu are with the School of Electronic and Information Engineering, South China University of Technology, Guangzhou 510640, China, and also with the State Key Laboratory of Millimeter Waves, Nanjing 210096, China (e-mail: liuxy@scut.edu.cn).

Y. Fan is with the School of Electronic and Information, Guangdong Polytechnic Normal University, 510665, China (e-mail: hnanfy@163.com).

M. M. Tentzeris is with the School of Electrical and Computer Engineering, Georgia Institute of Technology, Atlanta, GA 30332, USA (e-mail: etentze@ece.gatech.edu).

1536-1225 (c) 2016 IEEE. Personal use is permitted, but republication/redistribution requires IEEE permission. See http://www.ieee.org/publications_standards/publications/rights/index.html for more information.

This article has been accepted for publication in a future issue of this journal, but has not been fully edited. Content may change prior to final publication. Citation information: DOI 10.1109/LAWP.2016.2590477, IEEE Antennas and Wireless Propagation Letters

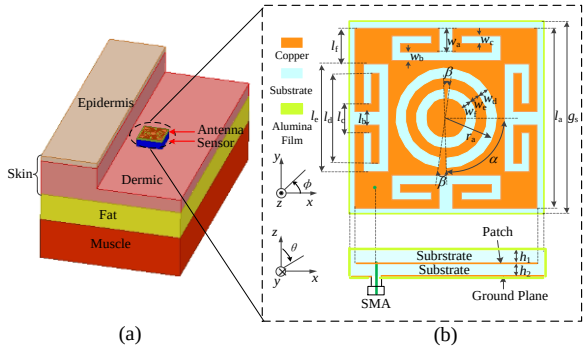

(a) (b)

Fig. 1. (a) Implantable medical device model, and (b) geometry of the proposed antenna.

TABLE I
OPTIMIZED ANTENNA DIMENSIONS

Parameter	Value	Parameter	Value	Parameter	Value
g_s	8.5 mm	w_a	1.05 mm	h_1	0.635 mm
l_a	8 mm	w_b	0.45 mm	h_2	0.635 mm
l_b	0.6 mm	w_c	0.35 mm	d_s	2 mm
l_c	1.3 mm	w_d	0.4 mm	α	90°
l_d	3.9 mm	w_e	0.5 mm	β	10°
l_e	4.8 mm	w_f	0.45 mm	--	--
l_f	1.6 mm	r_a	2.2 mm	--	--

The proposed antenna is fed through a 50-Ω coaxial cable with an inner conductor radius of 0.5 mm. In real implantable implementations, the whole antenna should be wrapped around by biocompatible materials to avoid shorting, while simultaneously alleviating the parasitic electromagnetic coupling with the surrounding human tissues. The presented prototype utilizes alumina (ε_r = 9.2, tan δ = 0.008) as the protecting film with a thickness of 0.02 mm, due to the fact that its permittivity is high and close to the dielectric of Rogers 3210. With the aid of ANSYS HFSS *v*.13, the optimized dimensions are obtained, as listed in Table I.

A three-layer phantom with a curved shape is constructed to mimic the typical human body. As depicted in Fig. 2(a), the tissue model consists of three layers, i.e., skin, fat, and muscle layers. Without loss of generality and despite the dispersive characteristics of the human tissues, the values of their electrical parameters, such as the relative permittivity and the conductivity, are tuned around the center frequency of 2.45 GHz to simplify computations. The proposed antenna is simulated in the above three-layer phantom with an implanted depth of d_s = 2 mm. As shown in Fig. 2(b), the proposed antenna has an impedance bandwidth of 12.2% (2.32–2.62 GHz) with S_{11} below -10 dB, and a 3-dB AR bandwidth of 2.4% (2.42–2.48 GHz). With reference to Fig. 3(a), a beamwidth from -70° to 70° in the *xz*- and *yz*- principal planes is obtained with AR below 3 dB. As can be easily observed in the radiation patterns at 2.45 GHz, shown in Fig. 3(b), the proposed antenna mainly radiates in the off-body direction and has a peak gain of -17 dBi at boresight. The negative gain is mainly due to the electrically small size of the proposed antenna and the high dissipation caused by the surrounding human tissues. Also, a right-handed circular polarization (RHCP) with a cross-polarization discrimination (XPD) of ~29.4 dB in the main radiation direction can be observed, thus revealing a high suppression over the

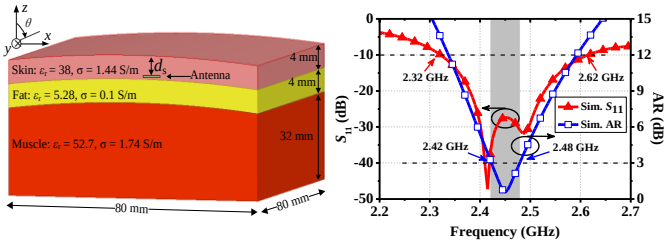

(a) (b)

Fig. 2. (a) Three-layer phantom in HFSS, and (b) simulated S_{11} and AR

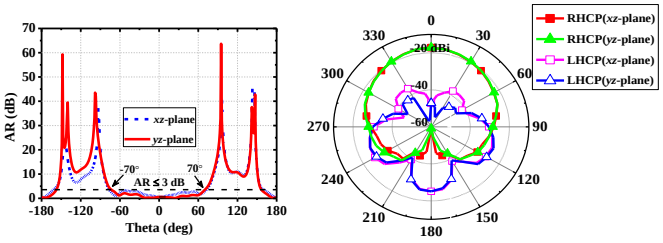

(a) (b)

Fig. 3. (a) Simulated AR in *xz*- and *yz*-planes at 2.45 GHz, and (b) simulated RHCP and LHCP radiation patterns at 2.45 GHz.

left-handed circular polarization (LHCP).

B. *Operating Mechanism*

1) Miniaturization of the Proposed Antenna: The proposed antenna has to be miniaturized due to the very limited space allowing to implant inside the human body. The miniaturization process is shown in Fig. 4. Initially, the proposed antenna is a conventional square-shaped patch antenna (case 1) on which the current path is relative short, resulting in the high resonant frequency of about 4.5 GHz. In order to lower the resonant frequency, four C-shaped slots surrounding the patch edges are etched out to increase the effective length of the current path (case 2). As the CSRR is one of the metamaterial structures that offer negative permeability values, the electrical length of this metamaterial unit cell is much smaller than the wavelength at the operation frequency [8]. Hence, a circular CSRR is loaded in the center of the patch (case 3) to further shift the resonant frequency down to about 2.45 GHz.

2) CP Realization: To be insensitive to orientation variations, two currents in orthogonal-in-space directions with a 90° out of time phase should be excited simultaneously to achieve a CP performance [11]. As illustrated in Fig. 5(a), when the CSRR is loaded in the middle of the radiator, at least two resonant frequencies are generated. With reference to Fig. 5(b)–(c), the directions of the current distributions at the first resonant frequency f_1 of 2.18 GHz and at the second resonant frequency f_2 of 2.4 GHz are normal to each other assuming that the SMA probe excitation is placed close to the bottom left corner (and in generally close to any corner) of the antenna. Through adjusting the geometrical parameters, such as r_a, α, and β of the slits in CSRR, f_1 and f_2 can get very close to 2.45 GHz, and then a time-phase shift of 90° between the two currents is introduced, thus enabling CP radiation characteristics.

Fig. 6 demonstrates the surface current distributions at 2.45 GHz in a period of *T*. By changing the time in steps of *T*/4, it can be observed that the direction of the composite current

1536-1225 (c) 2016 IEEE. Personal use is permitted, but republication/redistribution requires IEEE permission. See http://www.ieee.org/publications_standards/publications/rights/index.html for more information.

This article has been accepted for publication in a future issue of this journal, but has not been fully edited. Content may change prior to final publication. Citation information: DOI 10.1109/LAWP.2016.2590477, IEEE Antennas and Wireless Propagation Letters

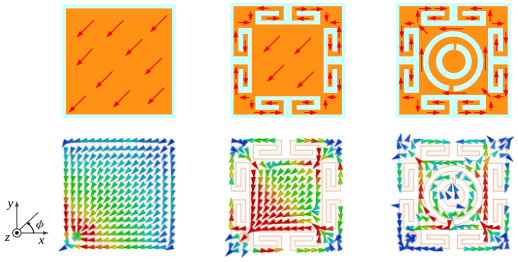

Fig. 4. Evolution of the proposed antenna topology along with the respective current distributions in (a) case 1, (b) case 2, and (c) case 3.

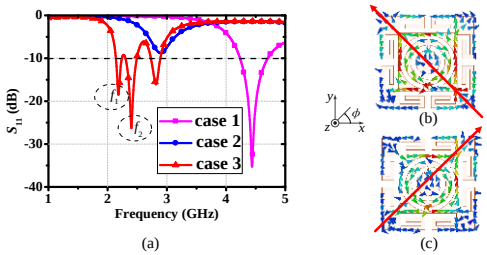

Fig. 5. (a) Simulated S_{11} for the three different cases shown in Fig. 4, (b) linear polarization along ϕ = 135° at 2.18 GHz, and (c) linear polarization along ϕ = 45° at 2.4 GHz.

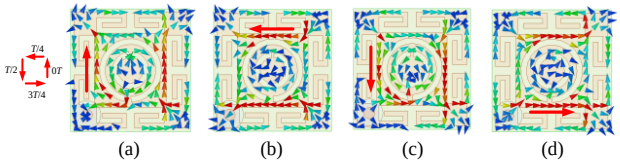

Fig. 6. Current distributions on the patch at (a) $t = 0T$, (b) $t = T/4$, (c) $t = T/2$, and (d) $t = 3T/4$.

distribution rotates in an anti-clockwise fashion, thus verifying the RHCP radiation, consistent with the results in Fig. 3.

3) Parametric Studies: To identify the main factors affecting the performance of the proposed antenna and to provide design guidelines, various key parameters are analyzed. Through the comparison of the simulation results shown in Fig. 7–9, it is clearly identified that the geometrical parameters, such as the radius r_a of the CSRR, the position α, and the size β of the slits, play a critical role in the input-impedance matching and in the surface-current distributions. Moreover, both S_{11} and AR are more sensitive to the changes of r_a than α and β. Hence, to efficiently optimize the structure, firstly r_a is coarsely tuned. As soon as the antenna performance characteristics get close enough to the design specifications, the values of α and β are finely adjusted, leading to an optimized 3-dB AR bandwidth from 2.42–2.48 GHz while allowing for a sufficient bandwidth with S_{11} lower than -10 dB.

C. Evaluation of the Radiation Safety Characteristics

To avoid the interference with existing wireless communication systems, the radiation power of the proposed antenna has to comply with the regulations of the equivalent isotropic radiated power (EIRP) of 36 dBm at ISM band, as specified by ITU [12]. Due to its significantly lower gain, the theoretical maximum input power of the proposed antenna can reach 200 W. Moreover, considering the health safety regulations, FCC restricts the maximum 1-g specific absorption rate (SAR) to 1.6

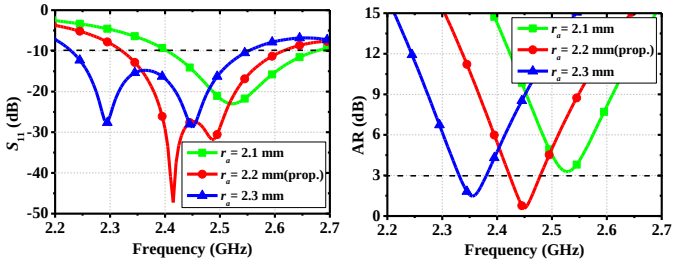

Fig. 7. Effect of varying r_a on (a) S_{11}, and (b) AR.

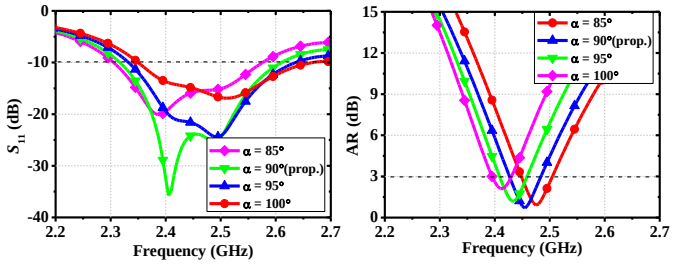

Fig. 8. Effect of varying slit position values α on (a) S_{11}, and (b) AR.

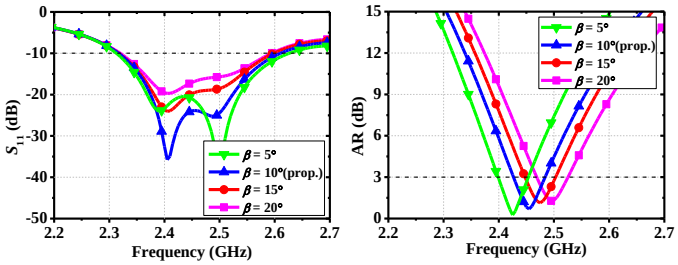

Fig. 9. Effect of varying slit size values β on (a) S_{11}, and (b) AR.

W/kg [13], leading through computations to a maximum allowable input power of 7.59 mW (8.8 dBm) to the proposed antenna in order to satisfy both SAR and EIRP standards.

III. Experimental Results and Analysis

A. In-Vitro Test Results

To experimentally verify the performance of the proposed antenna in implanted configurations, its performance was characterized by implanting it at the depth of d_m = 2 mm inside a slab of fresh streaky pork, composed of layers of skin, fat, and muscle, similar to the human phantom utilized in HFSS simulations. The photos of the fabricated prototype and of the experimental setup are demonstrated in Fig. 10. As shown in Fig. 11(a), the measured bandwidth covering the frequencies from 2.31 GHz to 2.63 GHz (13%) is consistent with the simulated results. The minor discrepancy between the measurements and the simulations could be attributed to fabrication and measurement tolerances. In addition, a linearly polarized half-wave dipole was employed as the external receiver to evaluate the CP performance of the proposed antenna. The dipole is placed at 100 mm right above the implanted antenna. The *S*-parameters between the dipole and the proposed antenna were measured when the dipole was oriented at phi = 0°, 45°, 90°, and 135°, respectively. With reference to Fig. 11(a), almost equal S_{21} with

1536-1225 (c) 2016 IEEE. Personal use is permitted, but republication/redistribution requires IEEE permission. See http://www.ieee.org/publications_standards/publications/rights/index.html for more information.

This article has been accepted for publication in a future issue of this journal, but has not been fully edited. Content may change prior to final publication. Citation information: DOI 10.1109/LAWP.2016.2590477, IEEE Antennas and Wireless Propagation Letters

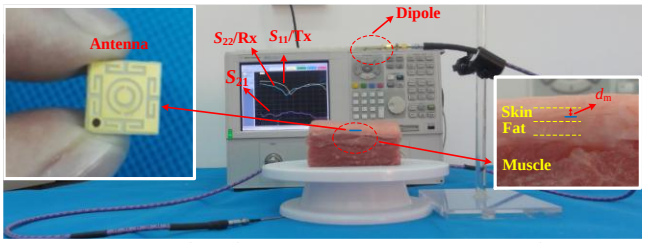

Fig. 10. Photograph of the fabricated antenna prototype and of the measurement setup.

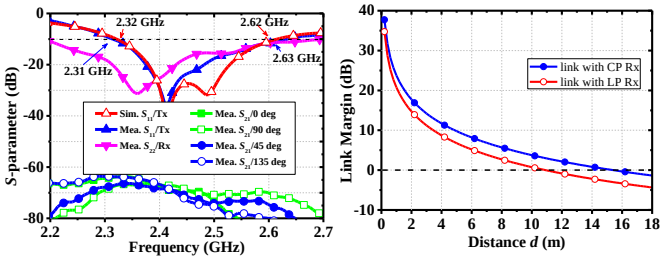

(a) (b)

Fig. 11. (a) Measured *S*-parameters, and (b) calculated link margin of the proposed CP implantable antenna.

a variation of less than 3 dB is obtained for all four orientations, confirming a high CP purity.

B. Characterization of the Communication Link

In order to evaluate the range of the data telemetry between the proposed antenna and a receiver outside the body, the communication link margin (LM) is investigated. The LM can be calculated as

$$\begin{aligned} LM\left(dB\right) &= \text{Link}\frac{C}{N_0} - \text{Required}\frac{C}{N_0} \\ &= P_{T_X} + G_{T_X} - P_L + G_{R_X} - L_f - N_0 \\ &\quad - \frac{E_b}{N_0} - 10\log_{10} B_r + G_c + G_d, \end{aligned} \tag{1}$$

where P_{Tx} is the transmitted power of the Tx antenna, G_{Tx} and G_{Rx} are the gains of the Tx and Rx antennas, respectively, P_L is the path loss and L_f is the feeding loss.

Various linearly and circularly polarized antennas with a realized gain of 2.15 dBi are introduced to work as the receiver, respectively. Assuming good matching, the loss caused by the impedance mismatch can be neglected, while the polarization mismatch losses can be ideally set to 3 dB and 0 dB with respect to linear and circular polarizations. The feeding power to the implantable antenna is chosen to be -40 dBm, which meets the above-mentioned safety requirements. The other associated parameter values used for the calculation of LM are chosen to be similar to those reported in the related literature [14]. As depicted in Fig. 11(b), the maximum communication range could be reached within 10 m for LM values larger than 0 dB.

IV. Conclusions

This letter has introduced a novel single-fed compact circularly polarized implantable antenna for biomedical applications at ISM band (2.40–2.48 GHz). The Table II provides a brief comparison of the proposed antenna with previous works. By employing four C-shaped slots and a loaded CSRR embedded inside the radiation patch, the proposed antenna features a peak gain of -17 dBi with the compact dimensions of 8.5 ×8.5 ×1.27 mm^3, while it can realize a circular polarization with a wide 3-dB AR beamwidth of 140°. The in-vitro measurement data exhibit a good agreement with the simulation results. The radiation of the proposed antenna satisfies the health safety regulations and enables acceptable wireless communication ranges, leading to numerous potential applications in real-time implantable biomonitoring, *e.g.*, transcutaneous glucose monitoring.

TABLE II
Comparison of the Proposed Antenna With Prior Art

Ref.	Implant Depth	Dimensions (mm ×mm ×mm)	Bandwidth (S_{11} < -10 dB)	Bandwidth (AR < 3 dB)	Peak Gain
[9]	4 mm in skin	10 ×10 ×1.27 (127 mm^3)	2.36–2.55 GHz (~7.74 %)	2.44–2.48 GHz (~1.63%)	-22 dBi
[10]	50 mm in muscle	π ×(5.5)^2 ×3.81 (~362 mm^3)	1.85–2.8 GHz (~38.7 %)	2.0–2.8 GHz (~32.6%)	-32 dBic
This work	2 mm in skin	8.5 ×8.5 ×1.27 (~92 mm^3)	2.32–2.62 GHz (~12.2%)	2.42–2.48 GHz (~2.4%)	-17 dBi

References

[1] T. Karacolak, A. Z. Hood, and E. Topsakal. "Design of a dual-band implantable antenna and development of skin mimicking gels for continuous glucose monitoring," *IEEE Trans. Microw. Theory Tech.*, vol. 56, no. 4, pp. 1001–1008, Apr. 2008.

[2] T. Yilmaz, R. Foster, and Y. Hao, "Broadband tissue mimicking phantoms and a patch resonator for evaluating noninvasive monitoring of blood glucose levels," *IEEE Trans. Antennas Propag.*, vol. 62, no. 6, pp. 3064–3075, Jun. 2014.

[3] P. S. Hall and Y. Hao, *Antennas and Propagation for Body-Centric Wireless Communications*, 2nd ed., Norwood, MA, USA: Artech House, 2012.

[4] A. Kiourti and K. S. Nikita, "A review of implantable patch antennas for biomedical telemetry: Challenges and solutions," *IEEE Antennas Propagat. Mag.*, vol. 54, no. 3, pp. 210–228, Jun. 2012.

[5] C. L. Yang, C. L. Tsai, and S. H. Chen, "Implantable high-gain dental antennas for minimally invasive biomedical devices," *IEEE Trans. Antennas Propag.*, vol. 61, no. 5, pp. 2380–2387, May 2013.

[6] H. Li, Y. X. Guo, C. Liu, S. Xiao, and L. Li, "A miniature-implantable antenna for medradio-band biomedical telemetry," *IEEE Antennas Wireless Propag. Lett.*, vol. 14, pp. 1176–1179, 2015.

[7] J. D. Baena, J. Bonache, F. Martin, R. M. Sillero, F. Falcone, T. Lopetegi, M. A. G. Laso, J. Garcia-Garcia, I. Gil, M. F. Portillo, and M. Sorolla, "Equivalent-circuit models for split-ring resonators and complementary split-ring resonators coupled to planar transmission lines," *IEEE Trans. Microw. Theory Tech.*, vol. 53, no. 4, pp. 1451–1461, Apr. 2005.

[8] X. Cheng, D. E, C. Kim, and Y. Yoon, "A compact omnidirectional self-packaged patch antenna with complementary split-ring resonator loading for wireless endoscope applications," *IEEE Antennas Wireless Propag. Lett.*, vol. 10, pp. 1532–1535, 2011.

[9] C. Liu, Y. X. Guo, and S. Xiao, "Capacitively loaded circularly polarized implantable patch antenna for ISM band biomedical applications," *IEEE Trans. Antennas Propag.*, vol. 62, no. 5, pp. 2407–2417, May 2014.

[10] C. Liu, Y. X. Guo, and S. Xiao, "Circularly polarized helical antenna for ISM-band ingestible capsule endoscope systems," *IEEE Trans. Antennas Propag.*, vol. 62, no. 12, pp. 6027–6039, Dec. 2014.

[11] K. Saurav, D. Sarkar, and K. V. Srivastava, "Dual-polarized dual-band patch antenna loaded with modified mushroom unit cell," *IEEE Antennas Wireless Propag. Lett.*, vol. 13, pp. 1357–1360, 2014.

[12] Rec. ITU-R M.1450-5, Int. Telecommun. Union, Geneva, Switzerland, 1998.

[13] Federal Communications Commission Rep. and Order (96-326), released Aug. 1, 1996.

[14] W. Xia, K. Saito, M. Takahashi, and K. Ito, "Performances of an implanted cavity slot antenna embedded in the human arm," *IEEE Trans. Antennas Propag.*, vol. 57, no. 4, pp. 894–899, Apr. 2009.

1536-1225 (c) 2016 IEEE. Personal use is permitted, but republication/redistribution requires IEEE permission. See http://www.ieee.org/publications_standards/publications/rights/index.html for more information.